

## Role of Silylene in the Pyrolysis of Silane and Organosilanes

J. J. O'Brien and G. H. Atkinson\*

Department of Chemistry and Optical Sciences Center, University of Arizona, Tucson, Arizona 85721

(Received: February 1, 1988)

The role of the silylene radical,  $\text{SiH}_2$ , in the pyrolytic decomposition of silane and organosilanes is examined. Silylene is detected directly in absorption by intracavity laser spectroscopy (ILS). This represents the first reported detection of  $\text{SiH}_2$  during the pyrolytic decomposition of silanes. The high detection sensitivity of ILS for absorption measurements enables the in situ examination of the pyrolytic decomposition processes under reaction conditions chosen to facilitate film growth rather than to optimize spectroscopic detection. The relative amount of gas-phase  $\text{SiH}_2$ , as measured by ILS data during chemical vapor deposition (CVD), correlates well with changes in the temperature and gas-flow rates in the pyrolysis chamber and with semiquantitative observations of the rate of film growth. These results demonstrate the importance of homogeneous reactions such as those involving  $\text{SiH}_2$  in the pyrolytic CVD of silicon films.

### Introduction

The need for studies of the molecular mechanism(s) that underlie the chemical vapor deposition (CVD) of silicon (Si) films is widely accepted. A detailed understanding of these processes at the molecular level can be of significant value in several areas associated with materials preparation, including the reduction of dimensions in semiconductor devices, the development of film deposition techniques that offer more precise control of film deposition processes in space and time (e.g., laser-assisted deposition), and the search for new source materials. In spite of this wide-ranging interest, many fundamental aspects of the CVD of Si films remain unknown, including the relative importance of homogeneous (gas phase) and heterogeneous (surface) reactions under specific reaction conditions.<sup>1-5</sup>

The absence of nonintrusive, experimental methods that permit the in situ, quantitative detection of reaction intermediates formed under CVD conditions that are optimized for quality film growth has been a major barrier to a more complete understanding of the chemistry involved in these processes. Such detection capabilities also provide real-time diagnostic methods for optimizing and maintaining processing conditions. Recently, it has been demonstrated that this experimental capability for real-time, in situ analysis of CVD processes can be obtained by using intracavity laser spectroscopy (ILS).<sup>6,7</sup>

Although pyrolytic CVD techniques have served as a basis for preparing Si-containing films in the very large scale integrated (VLSI) manufacture of semiconductors for the past two decades, the importance of gas-phase reactive species in the molecular mechanisms underlying these processes has become widely recognized only recently. In contrast, the importance of gas-phase reactive species in studies of plasma CVD processes was recognized from the outset of their utilization in the preparation of materials for electronic devices. A review of mechanistic studies of the CVD of silicon has been published recently.<sup>8</sup>

Gas-phase  $\text{SiH}_2$  has been postulated frequently as a primary precursor to film growth in the CVD of Si and a:Si-H from silane under homogeneous decomposition conditions.<sup>9,10</sup>  $\text{SiH}_2$  is known to insert readily into Si-H and Si-Si bonds in the gas phase,<sup>11</sup>

and it is assumed that insertion reactions of  $\text{SiH}_2$  with surface Si-H and Si-Si bonds result in an accumulation of Si-containing deposits during CVD processes.<sup>9</sup> Since the lowest energy gas-phase dissociation channel for silane forms  $\text{SiH}_2$ ,<sup>4</sup> this reaction usually is invoked as the first step in reaction schemes used in modeling the gas-phase chemistry associated with the CVD of Si films from silane (e.g., ref 12 and 13). Recently, there have been numerous experimental<sup>4,14,15</sup> and theoretical<sup>16-19</sup> studies directed at refining thermodynamic, kinetic, and spectroscopic data concerning  $\text{SiH}_2$ . Such data obtained from fundamental studies of silicon hydride reaction dynamics are necessary for developing and testing CVD models that are based on gas-phase fluid mechanics and chemical kinetics.<sup>12,13,20</sup> For example, recent studies have led to a significant revision of the heat of formation of  $\text{SiH}_2$ .<sup>14-18</sup> Reaction rates of  $\text{SiH}_2$  with  $\text{H}_2$ ,  $\text{D}_2$ ,  $\text{SiH}_4$ ,  $\text{Si}_2\text{H}_6$ ,  $\text{CH}_4$ , and  $\text{C}_2\text{H}_4$  also have been measured by using transient absorption and laser-induced fluorescence (LIF) techniques.<sup>21,22</sup> Fluorescence lifetimes for individual rotational levels of the electronically excited  $^1\text{B}_1(020)$  vibronic state of  $\text{SiH}_2$  have been found to vary widely from level to level and to range from  $<10$  ns to  $>1$   $\mu\text{s}$ .<sup>23,24</sup> These latter results are particularly important for studies that rely on LIF to obtain quantitative information on the relative concentration of  $\text{SiH}_2$  in different rovibronic levels.

Although the importance of results from fundamental studies in the formulation of models for CVD is obvious, their impact is yet to be fully realized. For example, it is of interest to note that the elaborate model of film growth developed by Coltrin et al.<sup>12,13</sup> has been tested by comparison of the predicted and experimentally observed values for the relative molecular density (as a function of experimental parameters such as the position above the substrate and temperature) of only one chemical species proposed to be an intermediate in the CVD process, namely,  $\text{Si}_2$ .<sup>25</sup>

(11) For example: Gaspar, P. P. In *Reactive Intermediates*; Jones, M., Moss, R. A., Eds.; Wiley: New York, 1985; Vol. 3, p 333.

(12) Coltrin, M. E.; Kee, R. J.; Miller, J. A. *J. Electrochem. Soc.* **1984**, *131*, 425.

(13) Coltrin, M. E.; Kee, R. J.; Miller, J. A. *J. Electrochem. Soc.* **1986**, *133*, 1206.

(14) Shin, S. K.; Beauchamp, J. L. *J. Phys. Chem.* **1986**, *90*, 1507.

(15) Berkowitz, J.; Greene, J. P.; Cho, H.; Ruscic, B. *J. Chem. Phys.* **1987**, *86*, 1235.

(16) Viswanathan, R.; Thompson, D. L.; Raff, L. M. *J. Chem. Phys.* **1984**, *80*, 4230.

(17) Ho, P.; Coltrin, M. E.; Binkley, J. S.; Melius, C. F. *J. Phys. Chem.* **1985**, *89*, 4647.

(18) Ho, P.; Coltrin, M. E.; Binkley, J. S.; Melius, C. F. *J. Phys. Chem.* **1986**, *90*, 3999.

(19) Gordon, M. S.; Gano, D. R.; Binkley, J. S.; Frisch, M. J. *J. Am. Chem. Soc.* **1986**, *108*, 2191.

(20) Breiland, W. G.; Coltrin, M. E.; Ho, P. *J. Appl. Phys.* **1986**, *59*, 3267.

(21) Jasinski, J. M. *J. Phys. Chem.* **1986**, *90*, 555.

(22) Inoue, G.; Suzuki, M. *Chem. Phys. Lett.* **1985**, *122*, 361.

(23) Engel, Y. M.; Levine, R. D.; Thoman, J. W.; Steinfeld, J. I.; McKay, R. I. *J. Chem. Phys.* **1987**, *86*, 6561.

(24) Thoman, J. W.; Steinfeld, J. I.; McKay, R. I.; Knight, A. E. W. *J. Chem. Phys.* **1987**, *86*, 5909.

(1) Robertson, R.; Hils, D.; Gallagher, A. *Chem. Phys. Lett.* **1984**, *103*, 397.

(2) O'Neal, H. E.; Ring, M. A. *Chem. Phys. Lett.* **1984**, *107*, 442.

(3) Purnell, J. H.; Walsh, R. *Chem. Phys. Lett.* **1984**, *110*, 330.

(4) Jasinski, J. M.; Estes, R. D. *Chem. Phys. Lett.* **1985**, *117*, 495.

(5) Robertson, R.; Gallagher, A. *J. Chem. Phys.* **1986**, *85*, 3623.

(6) O'Brien, J. J.; Atkinson, G. H. *Chem. Phys. Lett.* **1986**, *130*, 321.

(7) O'Brien, J. J.; Goldstein, N.; Atkinson, G. H. In *Laser Applications to Chemical Dynamics*; El-Sayed, M. A., Ed.; Proceedings of SPIE, 1987, p 87.

(8) Jasinski, J. M.; Meyerson, B. S.; Scott, B. A. *Ann. Rev. Phys. Chem.* **1987**, *38*, 109.

(9) Scott, B. A.; Plecenik, R. M.; Simonyi, E. E. *Appl. Phys. Lett.* **1981**, *39*, 73.

(10) For example: Scott, B. A.; Brodsky, M. H.; Green, D. C.; Kirby, P. B.; Plecenik, R. M.; Simonyi, E. E. *Appl. Phys. Lett.* **1980**, *37*, 725.

Under the pressure conditions ( $\approx 1$  atm) used in those experimental studies,  $\text{SiH}_2$  has not been observed by LIF.<sup>26</sup> Thus, the validation of the model relies on LIF measurements of  $\text{Si}_2$ , a species that appears in the latter stages of the proposed multistep (20–27 steps) reaction sequence and that can be formed only from secondary chemistry. A more stringent test of the model would be a comparison of the predicted and experimental molecular densities of a reaction intermediate produced in the first step of the proposed reaction scheme, e.g.,  $\text{SiH}_2$ .

In this paper, the real-time, in situ detection of  $\text{SiH}_2$  formed during the pyrolytic decomposition of  $\text{SiH}_4$  and two organosilanes (ethylsilane and *tert*-butylsilane) is reported for the first time. The decompositions were performed under conditions selected to facilitate the CVD of Si-containing films, and, as a consequence, the relative concentrations of  $\text{SiH}_2$  observed can be related directly to the processing conditions used for Si film growth. These results are discussed in terms of the role of the homogeneous decomposition of  $\text{SiH}_4$  under pyrolytic decomposition conditions.

### Experimental Section

The principles and experimental methodology underlying the quantitative detection of a species by ILS have been presented elsewhere,<sup>6,7,27–37</sup> and only a brief account is given here. Enhanced absorption sensitivity is obtained by placing the species of interest inside the optical resonator cavity of a longitudinally multimode laser (i.e., ILS laser). Absorptions by intracavity species having spectroscopic transitions within the spectral profile of the ILS laser constitute losses within the resonator. If the spectral widths of the absorption transitions are significantly narrower than the spectral distribution of the laser gain curve, these absorption losses are wavelength selective and alter the competition that occurs as the modes of the laser resonator cavity compete for the same gain centers.<sup>38</sup> Consequently, the absorption spectrum of the intracavity absorber is superimposed on the output of the ILS laser. The enhanced detection sensitivity obtained by ILS has been accounted for in terms of the intracavity mode competition.<sup>27–29,34</sup> Spectroscopic detection based on ILS is obtained by dispersing the output of the laser and observing the spectral profile at a well-defined time after the onset of ILS laser operation. This time interval is termed the generation time,  $t_g$ . It has been shown that within certain boundary conditions of absorption strength and  $t_g$  values, ILS can be used to obtain quantitative absorbance data that obey a Beer–Lambert relationship.<sup>27–31,33</sup> The averaged, time-resolved spectrum observed by ILS is given by

$$\ln [I_0(\nu)/I(\nu)] = k(\nu) \phi(\nu) N(l/L)ct_g \quad (1)$$

where  $I_0(\nu)$  is the intensity of the laser at spectral frequency  $\nu$  in the absence of intracavity absorption,  $I(\nu)$  is the intensity of the laser at frequency  $\nu$  when there is intracavity absorption at  $\nu$ ,  $k(\nu)$  is the intensity of the absorption line,  $\phi(\nu)$  is the normalized absorption line profile,  $N$  is the number density of the intracavity absorber, and  $(l/L)ct_g$  is the effective absorption path length ( $\mathcal{L}_{\text{eff}}$ ).

- (25) Ho, P.; Breiland, W. G. *Appl. Phys. Lett.* **1984**, *44*, 51.  
 (26) Ho, P., personal communication.  
 (27) Antonov, E. N.; Koloshnikov, V. G.; Mironenko, V. R. *Opt. Commun.* **1975**, *15*, 99.  
 (28) Stoeckel, F.; Melieres, M. A.; Chenevier, M. *J. Chem. Phys.* **1982**, *76*, 2191.  
 (29) Antonov, E. N.; Kachanov, A. A.; Mironenko, V. R.; Plakhotnik, T. V. *Opt. Commun.* **1983**, *46*, 126.  
 (30) Kachanov, A. A.; Plakhotnik, T. V. *Opt. Commun.* **1983**, *47*, 257.  
 (31) Melieres, M. A.; Chenevier, M.; Stoeckel, F. *J. Quantum Radiat. Transfer* **1984**, *33*, 337.  
 (32) Stoeckel, F.; Schuh, M. D.; Goldstein, N.; Atkinson, G. H. *Chem. Phys.* **1985**, *95*, 135.  
 (33) Goldstein, N.; Brack, T. L.; Atkinson, G. H. *Chem. Phys. Lett.* **1985**, *116*, 223.  
 (34) Stoeckel, F.; Atkinson, G. H. *Appl. Opt.* **1985**, *24*, 3591.  
 (35) Harris, T. D. In *Ultrasensitive Laser Spectroscopy*; Klier, D. S., Ed.; Academic: New York, 1983; pp 343–367.  
 (36) Atmanspacher, H.; Scheingraber, H.; Vidal, C. R. *Phys. Rev. A* **1985**, *32*, 254.  
 (37) Atkinson, G. H. In *Advances in Chemical Reaction Dynamics*; Rentzepis, P. M., Capellos, C., Eds.; Reidel: Dordrecht, 1986; pp 207–228.  
 (38) For example: Demtroder, W. *Springer Ser. Chem. Phys.* **1982**, *5*, 390–395.

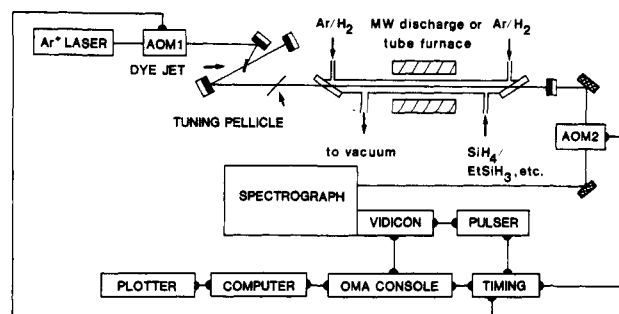


**Figure 1.** ILS spectrometer used to monitor gas-phase  $\text{SiH}_2$  produced during the CVD of Si-containing films by dissociation of silane, ethylsilane, and *tert*-butylsilane. The cavity of a broad-band dye laser has been extended to accommodate a CVD chamber. Two acousto-optic modulators (AOM1 and AOM2) are used to control the operation of the dye laser and the time at which its output is examined. AOM1 modulates the intensity of the  $\text{Ar}^+$  laser radiation reaching the dye jet above and below the threshold value required for dye laser operation. AOM2 diverts part of the ILS dye laser output beam into a spectrometer after the dye laser has operated for a well-defined period of time, the generation time ( $t_g$ ). The wavelength-dispersed radiation exiting the spectrometer is detected by an intensified vidicon camera. The various silanes are introduced to the CVD chamber via the port labeled  $\text{SiH}_4/\text{EtSiH}_3$ , etc., and are decomposed in the intracavity CVD chamber by pyrolysis in a tube furnace or by microwave discharge in an Evenson–Broida cavity.

The ratio  $l/L$  is the fraction of the laser resonator cavity occupied by the absorber, and  $c$  is the velocity of light. In practice,  $\mathcal{L}_{\text{eff}}$  values of  $\approx 100$  km have been realized by using ILS systems based on dye lasers (e.g., ref 27, 29, 24, 39, and 40).

The ILS spectrometer used to measure the absorption spectra of gas-phase species during the pyrolytic decomposition of silane and the organosilanes is shown schematically in Figure 1. Only major features of the instrumentation are described here since detailed descriptions have been provided elsewhere.<sup>6,32,33,37</sup>

The data reported here were obtained by using a quasi-continuous-wave (quasi-cw), broad-band dye laser (Coherent 590) that has been modified to accommodate a CVD chamber within its optical resonator cavity. Two acousto-optic modulators (AOM1 and AOM2) are used to control the operation of the dye laser and the time at which its output is examined. AOM1 modulates the intensity of the argon ion laser radiation reaching the dye jet above and below the threshold value required for dye laser operation. AOM2 diverts part of the ILS dye laser output beam into a spectrometer after the dye laser has operated for a well-defined period of time, i.e.,  $t_g$ . The wavelength-dispersed radiation exiting the spectrometer (McPherson Model 2051) is focused onto the face of a 500-channel, intensified vidicon camera (PARC Model 1205D SIT detector). The results of many repetitions ( $\approx 170$ ) of the dye laser operating cycle are summed and corrected for background signal in an optical multichannel analyzer (PARC Model 1205A). The wavelength of the dye laser is controlled throughout the lasing range of the dye used (rhodamine 6G, rhodamine 610, or rhodamine 560) by angle tuning an intracavity pellicle (uncoated). The spectral band width of the ILS system primarily depends on  $t_g$  and on the finesse of the pellicle and is typically 0.8 nm ( $22 \text{ cm}^{-1}$ ) for a  $t_g$  value of  $\sim 100 \mu\text{s}$ . The spectral resolution of the system is governed by the resolving power of the spectrometer and the pixel spacing of the detection system and is approximately 95 000 ( $0.18 \text{ cm}^{-1}$ ). Substantial portions of the rovibronic structure in the absorption spectrum of a species such as  $\text{SiH}_2$  can be monitored, therefore, in real time (acquisition time  $\approx 5$  s).

The intracavity CVD chamber, located within the 1-m-long optical cavity of the dye laser (150-MHz longitudinal mode spacing), is equipped with 12-mm-thick, wedged, fused silica windows positioned at Brewster's angle. During CVD processes,

- (39) Baev, V. M.; Belikova, T. P.; Ippolitov, M. B.; Sviridenkov, E. A.; Suchkov, A. F. *Opt. Spectrosc. (USSR)* **1978**, *45*, 31.  
 (40) Antonov, E. N.; Berik, E. B.; Koloshnikov, V. G. *J. Quantum Spectrosc. Radiat. Transfer* **1979**, *22*, 45.

the inner surfaces of these windows are continuously flushed with hydrogen ( $H_2$ ) or argon (Ar) to keep them free of any particulate products of the decomposition that would result in unacceptable optical losses for the laser cavity. The CVD chamber is demountable and consists of sections of quartz tubing joined together with stainless-steel fittings (Cajon Ultra-Torr). After each CVD run, the central 30-mm-long section of the chamber, which includes the zone where the decomposition and deposition processes occur, is replaced with a new and freshly cleaned quartz tube.

The various gases are introduced into the CVD chamber by using a stainless-steel gas handling system. A combination of rotameters with associated needle valves, a mass flow controller (Tylan Model FC-260), and a mass flow meter (Tylan Model FM-380) are used to control and measure gas-flow rates into the chamber. The chamber evacuation rate is regulated precisely during CVD processing by shutting off the main vacuum port and only pumping through a variable, low-conductance, bypass line equipped with a needle valve. Pressures are monitored with capacitance manometers.

Silane and the two organosilanes are decomposed in the intracavity chamber either (1) by pyrolysis in a 1500-W, 12-cm-long tube furnace that surrounds the central section of the CVD chamber or (2) by a microwave discharge in an Evenson-Broida cavity operated from a stabilized power supply at  $\approx 100$  W.<sup>41</sup> In both cases, the decomposition region is geometrically concentric with the optical axis of the ILS laser. In the microwave-driven plasma, species in excited states with energies up to the first ionization potential (IP) of the major gas component (IP(Ar) = 15.8 eV) can be observed.<sup>6</sup> In the pyrolysis chamber, there is a considerable variation in temperature along the axis of the chamber and hence along the path of the ILS laser. All the pyrolysis temperatures reported here ( $T_h$ ) refer to the temperatures recorded by a thermocouple affixed to the external wall of the chamber at the center of the hot zone. Temperatures of up to  $T_h = 1000$  °C are attainable in the tube furnace. In order to cool the chamber walls outside of the tube furnace, cold water is passed through copper tubing coiled around the quartz chamber wall and located on both sides of the tube furnace at a distance of 16 cm from the center of the hot zone. Measurements show that the temperature of the external wall decreases symmetrically with distance from the center of the hot zone. For example, for  $T_h = 500$ – $700$  °C, temperatures of the external wall at distances 2 and 6 cm from the center (and hottest part) of the chamber are 20 and 100–110 °C cooler, respectively. Furthermore, the temperature inside the pyrolysis chamber at a position corresponding to the middle of the hot zone is found to be 50–55 °C lower than  $T_h$  for  $T_h$  values of 500–700 °C and for chamber pressures of 6–120 Torr of  $H_2$ .

Argon (99.998% min purity), hydrogen (99.99% min purity), ethylsilane (Petrarch E6335), and silane (Linde, electronic grade) were used as received. *tert*-Butylsilane was prepared by reduction of *tert*-butyltrichlorosilane with  $LiAlH_4$  following the procedure for preparation of ethylsilane as described by Tannenbaum et al.<sup>42</sup> The *tert*-butylsilane samples were degassed by repeated freeze (liquid nitrogen)–pump–thaw cycles before use.

## Results and Discussion

Presented in Figure 2 are ILS spectral profiles obtained for the pyrolytic decomposition of silane in  $H_2$  at various temperatures ( $T_h = 620$ – $815$  °C). The spectral profiles presented in Figure 2 are in the wavelength region of the most intense spectroscopic transitions in the (020)'–(000)'' rovibronic band of  $SiH_2$ .<sup>43</sup> Although no notable absorption features are discernible in the profile obtained for  $T_h = 600$  °C (profile a), absorption features are evident for  $T_h > 650$  °C (profiles b and c). These comparisons are made for experiments in which the chamber pressure is kept constant. In general, the  $SiH_2$  absorption features increase in

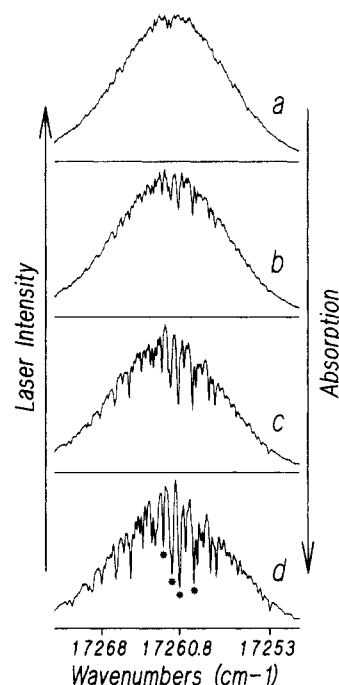


**Figure 2.** ILS spectral profiles for the pyrolytic decomposition of 30% silane in  $H_2$  at 6 Torr of total pressure and with  $T_h$  values of (a) 600, (b) 657, (c) 710, and (d) 813 °C ( $t_g = 125$   $\mu s$  for all four temperatures). The horizontal lines correspond to zero laser intensity. The features marked by asterisks are those monitored in obtaining the thermal profiles presented in Figure 5.

intensity as the pyrolysis temperature is increased.

A section of the ILS spectrum for the pyrolysis of silane obtained by combining several spectral profiles from adjacent (and overlapping) wavelength regions is presented in Figure 3. This spectrum also covers the spectral region where the strongest transitions of the (020)'–(000)'' band of  $SiH_2$  occur.<sup>43</sup> The assignment markers shown in Figure 3 for several rotational branches are derived from the work of Dubois.<sup>43</sup> These absorption data are in excellent agreement with ILS absorption spectra of  $SiH_2$  generated in the microwave-driven discharge of  $SiH_4$ .<sup>6</sup> Although all of the  $SiH_2$  absorption lines listed by Dubois<sup>43</sup> can be readily identified in the ILS spectrum, many additional absorption features are evident also. Even more absorption features are observed if the pyrolysis temperature is increased.

Presented in Figure 4 are ILS spectral profiles obtained for the pyrolytic decomposition of silane, ethylsilane, and *tert*-butylsilane under various temperature and pressure conditions. It is evident from these data that  $SiH_2$  is formed also during the pyrolysis of ethylsilane and *tert*-butylsilane and that the concentration of  $SiH_2$  produced is comparable to that produced during the pyrolysis of silane under similar conditions of temperature and pressure. As pyrolysis temperatures are varied, the ILS spectral profiles obtained during the pyrolysis of ethylsilane and *tert*-butylsilane show the same trend as observed in the pyrolytic decomposition of silane (Figure 2); specifically, the intensity of the  $SiH_2$  absorption features increase as the pyrolysis temperature is increased. For all three starting compounds, the relative intensities of the  $SiH_2$  absorption features increase as (1) temperature, (2) mole fraction of silicon source materials, and (3) residence time of the gas sample in the heated region of the sample cell increases. These trends are expected if  $SiH_2$  is a major reaction intermediate formed in the initial stages of the decomposition of each of these silanes.

Numerous studies<sup>27–31,33,35,36</sup> have shown that ILS can be used to perform quantitative absorption measurements by use of the relationship expressed by eq 1 provided that (1)  $t_g$  is chosen to ensure the unperturbed, temporal evolution of mode competition in a particular quasi-cw, multimode laser ( $t_g \leq 300$   $\mu s$ ), (2) the width of the absorption loss is substantially narrower than the bandwidth of the generation spectrum, (3) the ILS laser is operated close to threshold with a constant intracavity spectral power

(41) Atkinson, G. H.; McIlwain, M. E.; Venkatesh, C. G.; Chapman, D. M. *J. Photochem.* **1978**, *8*, 307.

(42) Tannenbaum, S.; Kaye, S.; Lewenz, G. F. *J. Am. Chem. Soc.* **1953**, *75*, 3753.

(43) Dubois, I. *Can. J. Phys.* **1968**, *46*, 2485. Dubois, I., Depository for Unpublished Data, National Science Library, Ottawa, Canada.

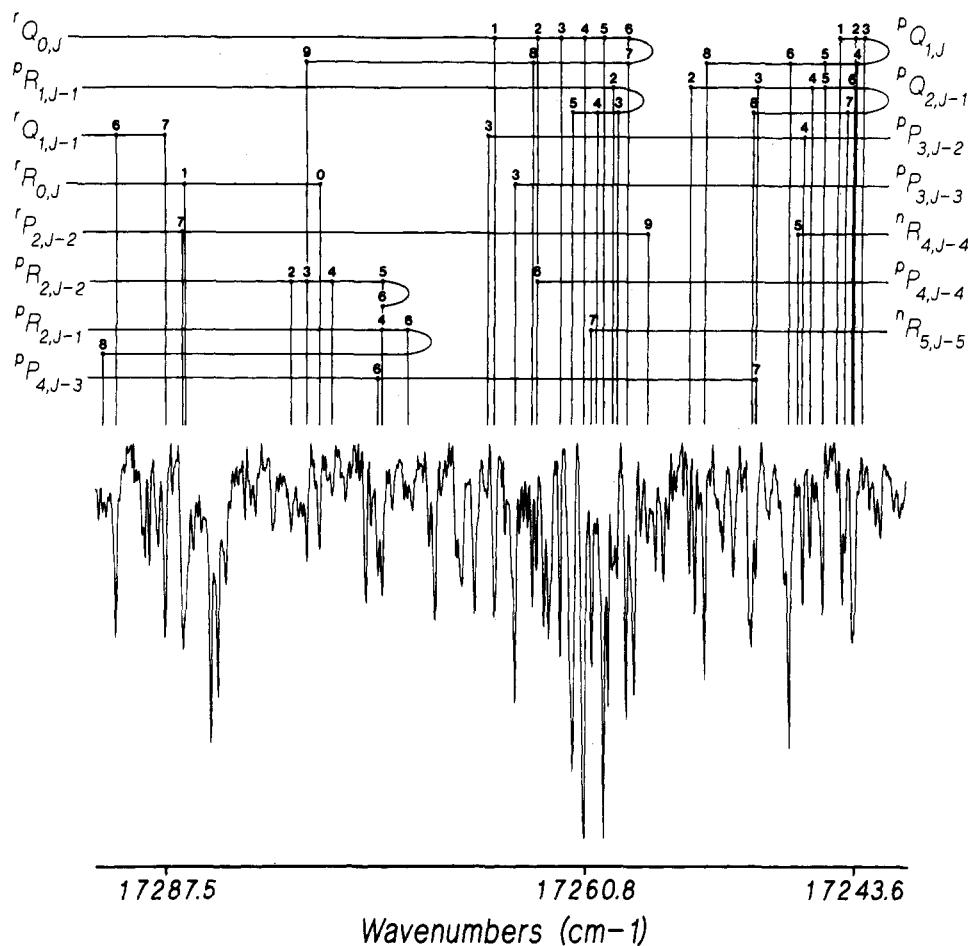


Figure 3. ILS spectrum for the pyrolysis of 31% silane in  $H_2$  at 5.9 Torr of total pressure and with  $T_h = 815^\circ C$  ( $t_g = 66 \mu s$ ). This spectrum is in the region of the strongest transitions of the  $(020)'-(000)''$  vibronic band of  $SiH_2$ . Assignment markers derive from the listing of Dubois.<sup>43</sup>

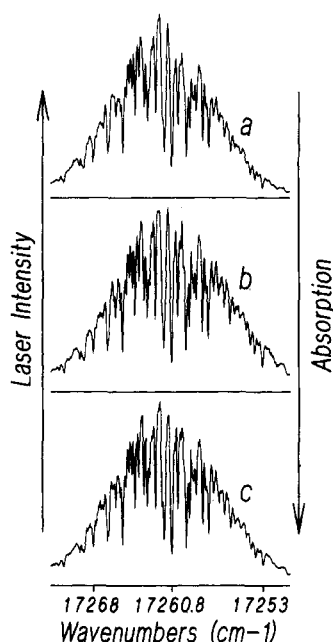


Figure 4. ILS spectral profiles for the pyrolysis of (a) 67% silane in  $H_2$  at 8.5 Torr of total pressure and with  $T_h = 856^\circ C$  ( $t_g = 135 \mu s$ ), (b) 16% ethylsilane in  $H_2$  at 8.7 Torr of total pressure and with  $T_h = 732^\circ C$  ( $t_g = 150 \mu s$ ), and (c) 14% *tert*-butylsilane in  $H_2$  at 7.3 Torr of total pressure and with  $T_h = 730^\circ C$  ( $t_g = 150 \mu s$ ). The horizontal lines correspond to zero laser intensity. The residence time of the gas in the hot zone of the CVD chamber was shorter for a than it was for b and c.

density, and (4) the relative strength of the absorption loss is small. Conditions 1–3 are fulfilled in the ILS data presented here, and, as a consequence, the relative concentration of  $SiH_2$  can be

monitored directly as a function of CVD conditions. There is some departure from the requirement described in condition (4) as the strength of the absorption features increase beyond  $I/I_0$  values of about 90%. This results in an underestimate of the concentration of the absorber, but is unavoidable if the other ILS parameters (e.g.,  $t_g$ ) are to be kept constant.

Of particular interest is the relative  $SiH_2$  concentration formed at various pyrolysis temperatures. The geometric arrangement of the ILS laser beam in the pyrolysis chamber and the dimensions of the oven itself limit the type of spatial information that can be derived from this measurement. Since there is a temperature gradient along the axis of the oven with the maximum temperature occurring near its center, it is reasonable to conclude that the concentration of  $SiH_2$  also exhibits a gradient. The passage of an ILS laser beam through the center of the pyrolysis chamber ensures that the entire concentration gradient is sampled. Since the absorption signals appearing in the ILS data are due to the total optical losses occurring along the entire intracavity path of the ILS laser, the  $SiH_2$  concentration measured by ILS is an integral of the  $SiH_2$  concentration gradient over this same intracavity optical path. Given these spatial constraints, the relative amount of  $SiH_2$  formed at pyrolytic temperatures ranging from 550 to 810  $^\circ C$  is presented in Figure 5. The peak heights of four rovibronic lines assigned to  $SiH_2$  and identified by asterisks in Figure 2 are used to monitor the relative  $SiH_2$  concentration. All of the absorption lines increase in strength with approximately the same dependence on the pyrolysis temperature.

Although film deposition rates were not measured quantitatively, qualitative indications of growth are provided by the rate at which discoloration and coating of the CVD quartz chamber wall occurs. From these indications, it is evident that the rate of film deposition increases as the intensities of the  $SiH_2$  absorption features increases. No significant film deposition occurs unless  $SiH_2$  is present at concentrations detectable by ILS.

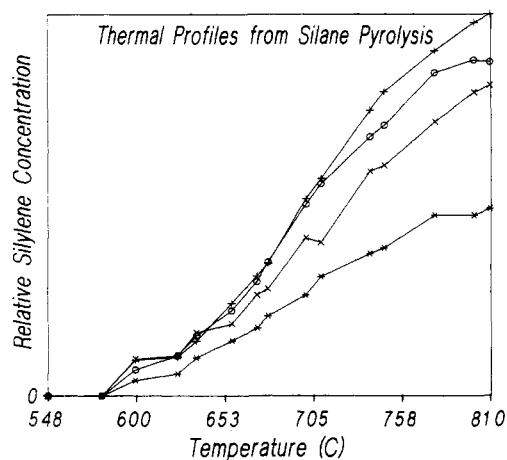


**Figure 5.** Thermal profiles for the pyrolysis of 31% silane in  $H_2$  at 5.9 Torr of total pressure. These curves were generated from ILS absorbance data for the four  $SiH_2$  absorption features denoted by asterisks in the spectrum presented in Figure 2. The assignments given by Dubois<sup>43</sup> to these transitions are  ${}^1Q_{0,J}(J=3)$  at  $17\,262.26\text{ cm}^{-1}$  (\*),  ${}^3P_{1,J-1}(J=5)$  at  $17\,261.70\text{ cm}^{-1}$  (x),  ${}^1Q_{0,J}(J=4)$  at  $17\,260.80\text{ cm}^{-1}$  (+), and  ${}^1Q_{0,J}(J=5)$  at  $17\,259.50\text{ cm}^{-1}$  (O). Relative  $SiH_2$  concentrations are determined by applying eq 1 to the absorbance data obtained for each temperature setting.

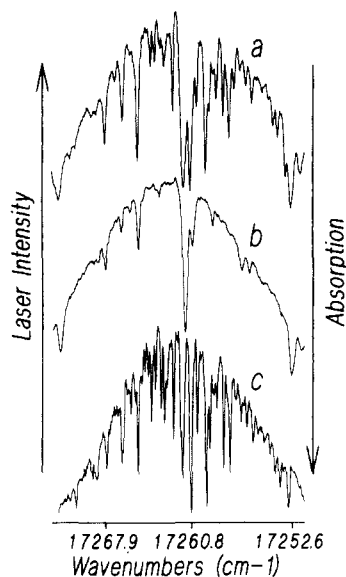


**Figure 6.** ILS spectral profiles indicating absorption features due to (a)  $SiH_2$ , electronically excited state  $H_2$  ( $H_2^*$ ), and Ar ( $t_g = 35\ \mu s$ ), (b)  $H_2^*$  and Ar ( $t_g = 45\ \mu s$ ), and (c)  $SiH_2$  ( $t_g = 61\ \mu s$ ). Profiles a and b were obtained for the microwave discharge of (1) 6%  $H_2$  in argon at 0.16 Torr of total pressure and (2) 1.2%  $SiH_4$  in argon at 1.1 Torr of total pressure, respectively. Profile c was obtained for the pyrolytic decomposition of 39% *tert*-butylsilane in  $H_2$  at 15.3 Torr of total pressure and with  $T_h = 725\ ^\circ C$ . The horizontal lines correspond to zero laser intensity.

We have reported previously the detection of  $SiH_2$  during the microwave discharge decomposition of silane in argon.<sup>6</sup> That study showed that electronically excited  $H_2$  ( $H_2^*$ ) also is observed by ILS in the plasma environment and that numerous absorption transitions of  $H_2^*$  occur in the region of the  $SiH_2$  (020)'-(000)'' band. In Figure 6, an ILS spectral profile obtained during the pyrolytic decomposition of *tert*-butylsilane in  $H_2$  (Figure 6c) is shown together with spectral profiles obtained for microwave discharges of silane in argon (Figure 6a) and of  $H_2$  in argon (Figure 6b). Comparison of the spectral profiles presented in Figure 6 indicates that (1) for the microwave discharge decomposition of silane, many of the  $H_2^*$  absorption features overlap absorption features probably assignable to  $SiH_2$  and (2) for the specific CVD conditions employed,  $SiH_2$  absorption features are more prominent in the spectral profiles obtained for pyrolytic decomposition conditions. It should be noted that under pyrolytic

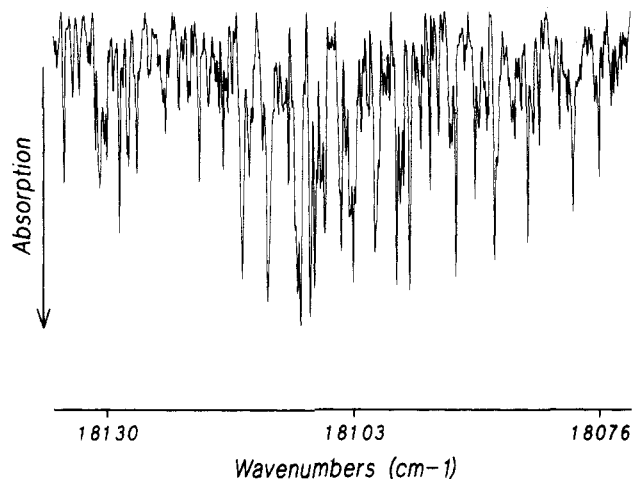


**Figure 7.** ILS spectrum for the pyrolysis of 52% silane in  $H_2$  at 8.5 Torr of total pressure and with  $T_h = 800\ ^\circ C$  ( $t_g = 125\ \mu s$ ). This spectrum is in the region of the strongest transitions of the (030)'-(000)'' band of  $SiH_2$ . The base line corresponds to zero laser intensity, i.e., 100% absorption.

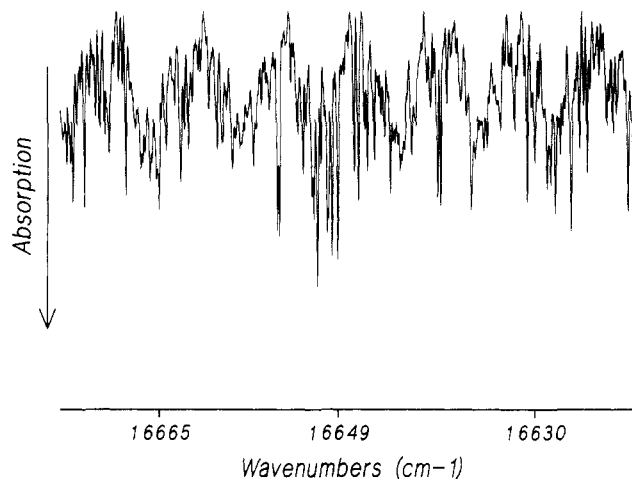


**Figure 8.** ILS spectrum for the pyrolysis of 26% ethylsilane in  $H_2$  at 5.1 Torr of total pressure and with  $T_h = 823\ ^\circ C$  ( $t_g = 132\ \mu s$ ). This spectrum is in the region of the strongest transitions of the (010)'-(000)'' vibronic band of  $SiH_2$ . The base line corresponds to zero laser intensity, i.e., 100% absorption.

decomposition conditions, there is no apparent mechanism for providing the 13–14-eV excitation energy required to promote  $H_2$  to the rovibronic states from which absorption transitions in the spectral region being monitored can occur, and consequently no absorption features assignable to  $H_2^*$  are observed in the spectrum presented in Figure 6c.

Absorption spectra for the (030)'-(000)'' (from silane pyrolysis) and (010)'-(000)'' (from ethylsilane pyrolysis) vibronic bands of  $SiH_2$  obtained by ILS are shown in Figures 7 and 8, respectively. All of the  $SiH_2$  transitions listed by Dubois<sup>43</sup> for these spectral regions can be identified among the ILS absorption features observed. There are, however, many additional absorption features in these ILS spectra that are yet to be assigned.

It is most likely that the unassigned absorption features observed in the ILS spectra (Figures 3, 6 and 7) presented here are due to  $SiH_2$ . Other workers<sup>44–46</sup> using both high-resolution absorption and fluorescence excitation techniques also have concluded that there are many lines in the region of the (020)'-(000)'' vibronic transition of  $SiH_2$  that were not reported by Dubois.<sup>43</sup> In all of these studies<sup>44–46</sup> and in the rotational analysis study performed by Dubois,<sup>43</sup>  $SiH_2$  was generated by photolysis of various silanes.

(44) Inoue, G.; Suzuki, M. *Chem. Phys. Lett.* **1984**, *105*, 641.

(45) Rayner, D. M.; Steer, R. P.; Hackett, P. A.; Wilson, C. L.; John, P. *Chem. Phys. Lett.* **1986**, *123*, 449.

(46) Jasinski, J. M.; Chu, J. O. *J. Chem. Phys.* **1988**, *88*, 1678.

The rotational temperature of SiH<sub>2</sub> generated under pyrolysis conditions is expected to be sufficiently different from that for SiH<sub>2</sub> generated by photolysis techniques to yield a different distribution of absorption lines. A study undertaken to examine these points is in progress.

### Concluding Remarks

ILS data have been presented that demonstrate that gaseous SiH<sub>2</sub> is produced during the pyrolytic decomposition of silane, ethylsilane, and *tert*-butylsilane. Frequently, SiH<sub>2</sub> has been postulated as an important gas-phase precursor to film formation in the CVD of Si from silane.<sup>9</sup> Kinetic studies have shown that the dominant dissociation channel for the homogeneous pyrolysis of silane must be the formation of SiH<sub>2</sub> + H<sub>2</sub>.<sup>4,9</sup> The data presented here, however, are the first direct evidence for the production of gas-phase SiH<sub>2</sub> by the pyrolytic decomposition of silane. Furthermore, the high detection sensitivity afforded by ILS enabled the direct, in situ detection of SiH<sub>2</sub> under CVD pyrolysis conditions that result in film growth at moderate temperatures and pressures.

Although film deposition rates were not measured quantitatively, several qualitative observations indicate that gaseous SiH<sub>2</sub> is a species that correlates directly with silicon film growth: (1) the concentration of SiH<sub>2</sub> averaged over the optical path of the ILS laser through the CVD chamber increases with pyrolysis temperature, (2) film deposition rates (as determined by the rate at which visible discoloration of the CVD chamber wall occurred) are faster for higher, relative concentrations of gaseous SiH<sub>2</sub>, (3) episodes of gas-phase nucleation (during which aggregation occurring in the gas phase results in the formation of a fine, gray powdery material) are preceded by very large increases in the intensity of SiH<sub>2</sub> absorption features, and (4) film deposition is negligible under conditions where SiH<sub>2</sub> is not detectable by ILS.

The ILS results also demonstrate that the pyrolytic decompositions of ethylsilane and *tert*-butylsilane involve the formation of SiH<sub>2</sub>. It is not possible to determine whether or not SiH<sub>2</sub> is

produced in the primary dissociation of these molecules from the ILS data presented here. The relative concentrations of SiH<sub>2</sub> produced in the pyrolysis of ethylsilane and *tert*-butylsilane, however, are comparable with those produced in the pyrolysis of silane under similar CVD conditions. This suggests that the formation of SiH<sub>2</sub> is a dominant reaction path for the decomposition of these organosilanes under the pyrolysis conditions examined. These results also indicate that ethylsilane and *tert*-butylsilane are good source materials for the pyrolytic CVD production of Si-containing films. It should be noted, however, that the CVD films obtained by the pyrolytic decomposition of ethylsilane and *tert*-butylsilane contain substantial amounts of carbon.<sup>47</sup> ESCA determinations show that the carbon fraction varies from 20% to 50% depending on the CVD conditions employed.<sup>47</sup>

The importance of homogeneous processes in pyrolytic CVD processes has often been underestimated. The results presented here indicate that the radical SiH<sub>2</sub> is an important intermediate in the pyrolytic decomposition of silane, ethylsilane, and *tert*-butylsilane at moderate temperatures and pressures. These results also illustrate the real-time, in situ, diagnostic capabilities that ILS can provide for quantitatively monitoring CVD processes in which gas-phase chemical reactions are important. For cases where gas-phase reactions play a significant role in CVD chemistry, such diagnostic capabilities can be used to optimize particular CVD processes and to evaluate different source materials.

*Acknowledgment.* We gratefully acknowledge Dr. Arthur Barry's assistance in the preparation of *tert*-butylsilane. This work was partially supported by a grant from the IBM Corp.

*Registry No.* SiH<sub>4</sub>, 7803-62-5; SiH<sub>2</sub>, 13825-90-6; ethylsilane, 2814-79-1; *tert*-butylsilane, 18165-85-0.

(47) O'Brien, J. J.; Barry, A. J.; Miller, D.; Atkinson, G. H. *Replacement of Silicon Tetrahydride (SiH<sub>4</sub>) in Chemical Vapor Deposition Reactions Used in VLSI Semiconductor Manufacturing*; Final Report, IBM Corp., 1987.

## Films of Amphiphiles: Packing Constraints and Phase Diagrams

J. Charvolin\* and J.-F. Sadoc

*Laboratoire de Physique des Solides, Associé au CNRS, Bât. 510, Université Paris-Sud, 91405 Orsay, France*  
(Received: February 8, 1988; In Final Form: April 21, 1988)

The polymorphism of systems of amphiphilic molecules in liquid crystalline and micellar regions of their phase diagrams is characterized by similar sequences of phases, whatever the details of the chemical structures of the molecules. For instance, varying the dominant parameter of the phase diagram and starting from a lamellar phase, the most general sequence continues with cubic and/or cylindrical phases and ends with micellar phases, each step of the sequence being characterized by a dramatic change of the topology of the organization of the molecules. As this behavior is independent of the chemical details of the amphiphilic molecules, it must be related to their common property of building interfaces organized in symmetric films. We have therefore applied our recent analysis of systems of amphiphiles as periodic systems of frustrated fluid films to this problem. We recall that, in our view, a frustration arises from the fact that symmetric interfacial curvatures different from zero and constant interfacial distances are not compatible in Euclidean space. In our preceding papers we demonstrated that the observed structures can be understood as the geometrical configurations adopted by the systems to optimize the frustration, i.e., to conciliate the two constraints, by spontaneous creations of disclinations. We now examine the properties of these geometrical configurations in detail. We show that, for each of them, any interfacial curvature cannot be fitted with any interfacial distance. They are indeed related by specific functions in each case, and the set of these relations is such that the configurations must appear along the sequence described above when the frustration varies with the parameters of the phase diagrams.

### Introduction

An examination of the literature concerning phase diagrams<sup>1</sup> and structures<sup>2</sup> of amphiphile/water systems imposes the idea of

a constant behavior whatever the details of the chemical structures of the amphiphilic molecules: similar structures appear along similar sequences when the dominant parameters of the phase diagrams are varied. This is illustrated in Figure 1, where two

(1) Ekwall, P. *Adv. Liq. Cryst.* 1975, 1, 1.

(2) Luzzati, V. *Biol. Membr.* 1968, 1, 71.